

28 Apr 2023

## From Fiber Bragg Gratings To Coaxial Cable Bragg Gratings: One-dimensional Microwave Quasi-periodic Photonic Crystals

Chen Zhu

*Missouri University of Science and Technology, cznwq@mst.edu*

Osamah Alsalman

Jie Huang

*Missouri University of Science and Technology, jieh@mst.edu*

Follow this and additional works at: [https://scholarsmine.mst.edu/ele\\_comeng\\_facwork](https://scholarsmine.mst.edu/ele_comeng_facwork)



Part of the [Electrical and Computer Engineering Commons](#)

---

### Recommended Citation


C. Zhu et al., "From Fiber Bragg Gratings To Coaxial Cable Bragg Gratings: One-dimensional Microwave Quasi-periodic Photonic Crystals," *Journal of Applied Physics*, vol. 133, no. 16, article no. 164503, American Institute of Physics, Apr 2023.

The definitive version is available at <https://doi.org/10.1063/5.0148559>

This Article - Journal is brought to you for free and open access by Scholars' Mine. It has been accepted for inclusion in Electrical and Computer Engineering Faculty Research & Creative Works by an authorized administrator of Scholars' Mine. This work is protected by U. S. Copyright Law. Unauthorized use including reproduction for redistribution requires the permission of the copyright holder. For more information, please contact [scholarsmine@mst.edu](mailto:scholarsmine@mst.edu).

RESEARCH ARTICLE | APRIL 24 2023

# From fiber Bragg gratings to coaxial cable Bragg gratings: One-dimensional microwave quasi-periodic photonic crystals

Chen Zhu  ; Osamah Alsaman ; Jie Huang

 Check for updates

*Journal of Applied Physics* 133, 164503 (2023)

<https://doi.org/10.1063/5.0148559>

  
View  
Online

  
Export  
Citation

 CrossMark

## Articles You May Be Interested In

Coaxial cable Bragg grating

*Appl. Phys. Lett.* (September 2011)

Control of critical coupling in a coiled coaxial cable resonator

*Rev Sci Instrum* (May 2014)

Two-slot coiled coaxial cable resonator: Reaching critical coupling at a reduced number of coils

*Rev Sci Instrum* (November 2014)

Downloaded from [http://pubs.aip.org/aip/jap/article-pdf/doi/10.1063/5.0148559/1696833/164503\\_1\\_5.0148559.pdf](http://pubs.aip.org/aip/jap/article-pdf/doi/10.1063/5.0148559/1696833/164503_1_5.0148559.pdf)



Time to get excited.  
Lock-in Amplifiers – from DC to 8.5 GHz

[Find out more](#)

 Zurich  
Instruments

# From fiber Bragg gratings to coaxial cable Bragg gratings: One-dimensional microwave quasi-periodic photonic crystals

Cite as: J. Appl. Phys. 133, 164503 (2023); doi: 10.1063/5.0148559

Submitted: 1 March 2023 · Accepted: 9 April 2023 ·

Published Online: 24 April 2023



Chen Zhu,<sup>1,a)</sup> Osamah Alsalman,<sup>2</sup> and Jie Huang<sup>3</sup>

## AFFILIATIONS

<sup>1</sup>Research Center for Optical Fiber Sensing, Zhejiang Laboratory, Hangzhou 311100, China

<sup>2</sup>Department of Electrical Engineering, College of Engineering, King Saud University, P.O. Box 800, Riyadh 11421, Saudi Arabia

<sup>3</sup>Department of Electrical and Computer Engineering, Missouri University of Science and Technology, Rolla, Missouri 65409, USA

<sup>a)</sup>Author to whom correspondence should be addressed: [chenzhu@zhejianglab.com](mailto:chenzhu@zhejianglab.com)

## ABSTRACT

Coaxial cables and optical fibers are two types of cylindrical waveguides used in telecommunications. Fiber Bragg gratings (FBGs) have found successful applications in various fields, such as optical communications, fiber lasers, and fiber-optic sensing. In this paper, we propose and numerically investigate the implementations of various fiber Bragg configurations, including uniform, chirped, apodized, and phase-shifted configurations, on coaxial cables to generate the corresponding special types of coaxial cable Bragg gratings (CCBGs). The simulation results of different CCBGs match well with the well-known FBG theories. It is demonstrated that the reflection spectrum of a CCBG can be flexibly tailored by introducing various quasi-periodic perturbations in the permittivity of the dielectric layer along the coaxial cable. The proposed special types of CCBGs with unique characteristics could find potential applications in radio frequency signal processing, communication, and sensing fields.

Published under an exclusive license by AIP Publishing. <https://doi.org/10.1063/5.0148559>

## I. INTRODUCTION

Over the years, optical fibers have revolutionized the telecommunication fields, making high-speed, high-quality, and large-capacity long-haul signal transmission realized.<sup>1</sup> In addition to telecommunication applications, several unique fields based on optical fibers have been developed due to the advancements in optical fiber manufacturing and micromachining techniques, including fiber-optic sensors,<sup>2</sup> fiber lasers,<sup>3</sup> and fiber amplifiers.<sup>4</sup> Fiber Bragg gratings (FBGs) have played a significant role in these fields.<sup>5–8</sup> An FBG is typically manufactured by introducing periodic perturbations in the refractive index of the fiber core using optical methods, such as UV laser exposure<sup>9</sup> and ultrafast laser micromachining.<sup>10</sup> The periodic grating structure acts as a mirror to the optical signals propagating in the fiber core, where those waves with wavelengths satisfying the Bragg condition will be selectively reflected and the others will transmit. The Bragg wavelength ( $\lambda_B$ ) can be expressed as<sup>6</sup>

$$\lambda_B = 2n_{eff}\Lambda, \quad (1)$$

where  $n_{eff}$  is the effective refractive index in the fiber core and  $\Lambda$  is the grating period. The properties of an FBG, i.e., Bragg wavelength, reflectivity, reflection bandwidth, and the sidelobe strength, are uniquely determined by the variations of induced index changes in the fiber core along the axial direction, including the grating period, the grating length, and also the strength of the refractive index modulation. Generally, FBGs can be divided into two categories, uniform and non-uniform gratings. The grating period or the induced refractive index change of non-uniform gratings varies at different locations along the fiber axial direction. Examples include chirped, apodized, phase-shifted, and superstructure FBGs. Figure 1 illustrates the common types of FBGs, where the induced index changes ( $\Delta n$ ) are plotted as a function of axial positions in the fiber core.<sup>5</sup> These different types of FBGs have been employed in various applications, including wavelength division multiplexing, add-drop filters, signal conditioners, chromatic dispersion compensation, high-reflective laser mirrors, and single-point or quasi-distributed sensing.<sup>9</sup>

In recent years, FBGs have found another successful application in structural health monitoring (SHM) for strain distribution

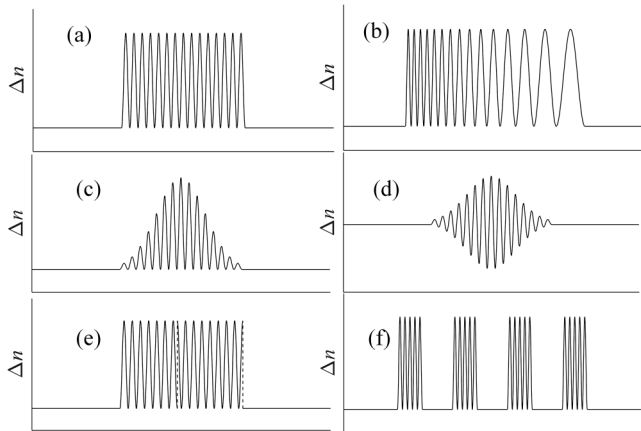


**FIG. 1.** Common types of FBG including (a) uniform, (b) period chirped, (c) Gaussian-apodized, (d) raised-cosine-apodized zero-dc index change, (e)  $\pi$  phase-shifted, and (f) superstructure.

mapping. Compared to traditional strain gauges, FBG-based strain sensors are embeddable, highly sensitive with high resolution, capable of remote operation and multiplexing, and immune to electromagnetic interference.<sup>11,12</sup> However, one challenge always exists in the fiber sensor packaging and installation in real-world harsh-environment scenarios, because optical fibers are generally fragile and can easily break under a shear force or a large strain (e.g.,  $>7000 \mu\epsilon$ ).<sup>13</sup> Several solutions were proposed to address this issue. Among them, the coaxial cable Bragg grating (CCBG) provided a viable solution for SHM applications with large strain capability, up to  $50\,000 \mu\epsilon$ .<sup>14,15</sup> Coaxial cables are another type of waveguide widely used in telecommunications, governed by the same electromagnetic (EM) theory as optical fibers. However, the frequencies supported by them are quite different, i.e., radio frequency (e.g., GHz) and optical frequency (e.g., THz). Over the years, the two waveguides have evolved along quite different paths. Compared to an optical fiber, a coaxial cable is larger in diameter and much more robust. Inspired by the well-known FBGs, the uniform CCBG was proposed as a strain-sensing device with large strain capability. The prototype CCBG was manufactured by introducing periodic impedance discontinuities into a commercial coaxial cable via hole-drilling methods.<sup>14,15</sup> Due to the coupling between the forward propagating wave and backward propagating wave, resonances were observed at discrete frequencies. Similarly, the resonant frequencies follow the Bragg condition,<sup>15</sup>

$$f_{res} = \frac{mc}{2\Lambda\sqrt{\epsilon_r}}, \quad (2)$$

where  $c$  is the speed of light in vacuum,  $\epsilon_r$  is the relative permittivity of the dielectric layer in the coaxial cable, and  $m$  is an integer denoting the resonant order. Using the CCBG as a sensor, external tensile strains were correlated to the resonant

frequency of the device, according to Eq. (2), as the grating period and the relative permittivity of the dielectric would change with strain variations.

In this paper, we further investigate the implementation of the FBG concept to coaxial cables, i.e., special types of CCBG. Different types of non-uniform CCBG are proposed and numerically studied using the coupled mode theory, including chirped, apodized, and phase-shifted. The potential applications of these special types of CCBGs are also discussed.

## II. COUPLED MODE THEORY-BASED MODELING

In previous studies about uniform CCBGs, different methods were employed for modeling the new device, including transmission line theory,<sup>15</sup> transfer matrix method,<sup>14</sup> and coupled mode theory.<sup>16</sup> The transmission line theory-based modeling was intuitive and useful for predicting the resonant frequencies of the device; the transfer matrix method offered an easy way to numerically investigate the reflection and transmission spectra of the device. However, when it comes to more complicated structures, i.e., non-uniform structures, these two methods are not applicable. In this paper, the coupled mode theory-based approach was employed.

Generally, a coaxial cable is designed for transmitting EM waves in transverse EM (TEM) mode. Therefore, only the coupling between forward and backward TEM waves is considered in the modeling. The coupled wave equation can be expressed as

$$\begin{cases} \frac{dA_1}{dz} = -jK(A_1 + A_2e^{j2\beta z}), \\ \frac{dA_2}{dz} = jK(A_1e^{-j2\beta z} + A_2), \end{cases} \quad (3)$$

where  $A_1$  and  $A_2$  are the amplitude of the forward and backward waves,  $\beta$  is the propagation constant of the TEM wave,  $z$  is the spatial position along the axial direction of the cable,  $K$  is the coupling coefficient between the forward and backward waves and is given by

$$K = \omega \iint_S dx dy \Delta\epsilon(x, y, z) |\overline{E(x, y)}|^2, \quad (4)$$

where  $x$  and  $y$  define the cross section plane of the cable at position  $z$ ,  $\omega$  is the angular frequency of the TEM wave,  $\Delta\epsilon(x, y, z)$  is the local change in the permittivity of the cable, and  $E(x, y)$  is the modal electric field at the cross section plane. The transfer matrix method

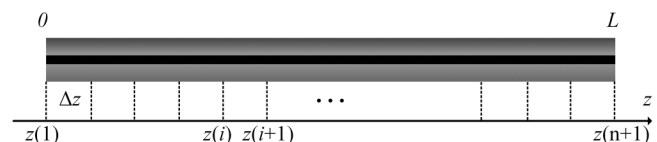


**FIG. 2.** Schematic of segmentation of a coaxial cable with a length of  $L$  along the axial direction, i.e.,  $z$ -direction.

Downloaded from http://pubs.aip.org/jap/article-pdf/doi/10.1063/5.0148559/1696633/164503\_1\_5.0148559.pdf

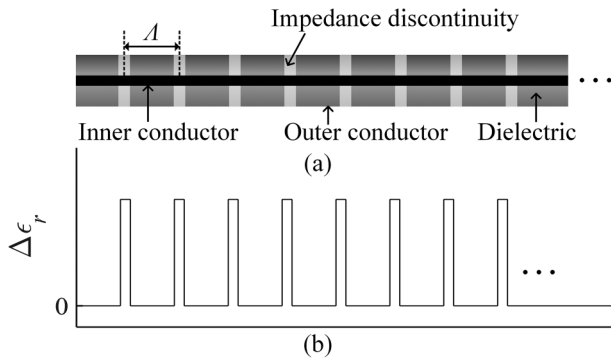


**FIG. 3.** Illustration of a uniform CCBG. (a) Schematic of periodic impedance discontinuities along a coaxial cable. (b) Change in relative permittivity with respect to spatial position along the axial direction of the cable.

based on a finite-difference analysis is employed to solve the coupled wave equation. Assume the entire coaxial cable with a length of  $L$  is segmented into  $n$  sections each with a length of  $\Delta z$ , as schematically shown in Fig. 2. The transfer matrix of the EM

waves at positions  $z(i)$  and  $z(i + 1)$  is given by

$$\begin{bmatrix} A_{1,i+1} \\ A_{2,i+1} \end{bmatrix} = F_i \begin{bmatrix} A_{1,i} \\ A_{2,i} \end{bmatrix} = \begin{bmatrix} -jK(i)\Delta z + 1 & -jK(i)e^{2j\beta z(i)}\Delta z \\ jK(i)e^{-2j\beta z(i)}\Delta z & jK(i)\Delta z + 1 \end{bmatrix} \cdot \begin{bmatrix} A_{1,i} \\ A_{2,i} \end{bmatrix}. \quad (5)$$

Therefore, the final transfer matrix of an arbitrary grating modified coaxial cable device can be derived as

$$F = F_n \cdot F_{n-1} \cdot \dots \cdot F_1 = \begin{bmatrix} F_{11} & F_{12} \\ F_{21} & F_{22} \end{bmatrix}. \quad (6)$$

Subsequently, the reflection spectrum ( $S_{11}$ ) of the device, defined as the ratio of the reflected wave to the incident wave at the input Port 1, can be calculated by

$$S_{11} = -\frac{F_{21}}{F_{22}}. \quad (7)$$

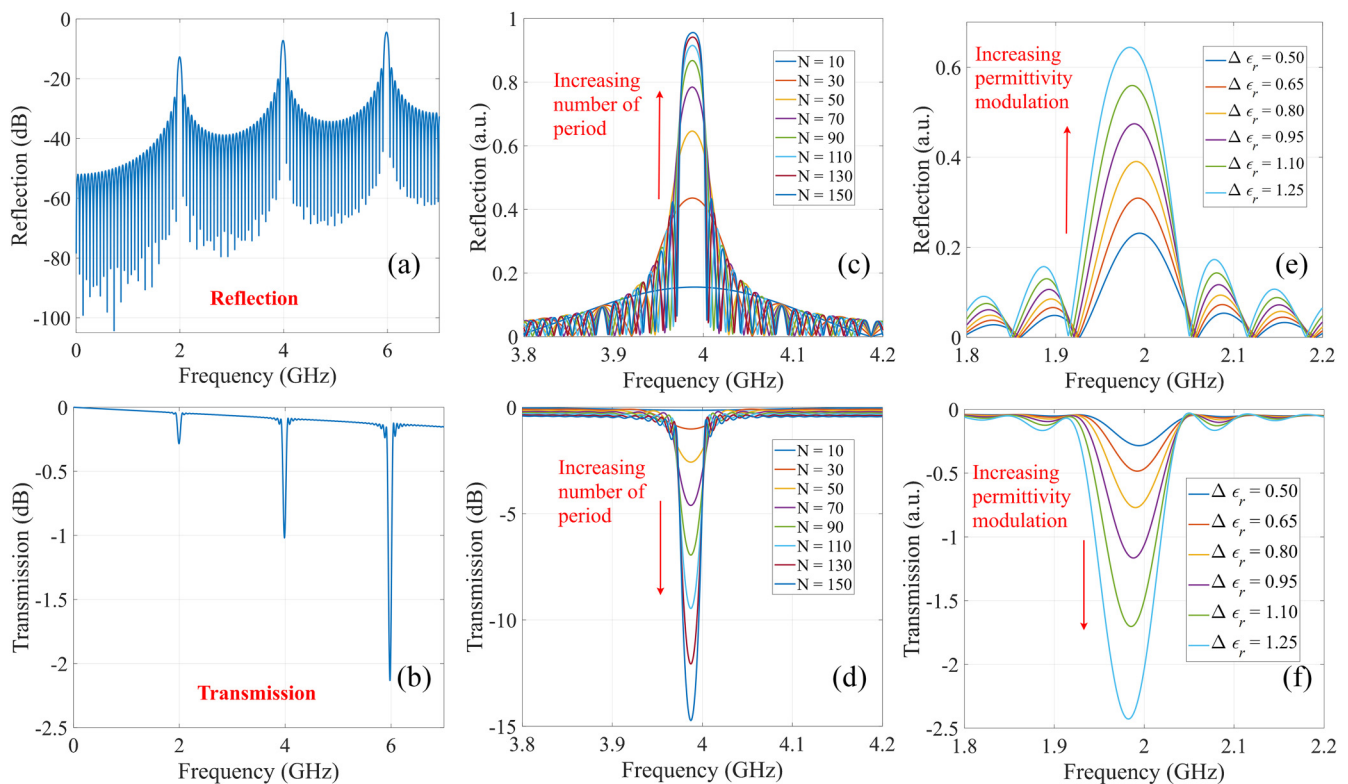


**FIG. 4.** Numerical investigation of uniform CCBGs. (a) Reflection and (b) transmission spectra of a CCBG device with 30 periods. (c) Reflection spectra and (d) transmission spectra of CCBGs with different numbers of periods. (e) Reflection spectra and (f) transmission spectra of CCBGs with different strengths of relative permittivity change in impedance discontinuities.

Downloaded from http://pubs.aip.org/jap/article-pdf/doi/10.1063/5.0148559/1696833/1.64503\_1\_5.0148559.pdf

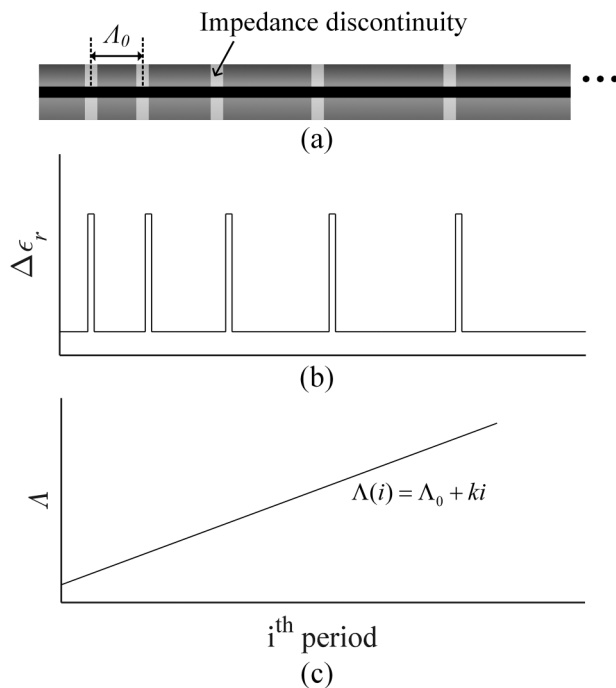


**FIG. 5.** Illustration of a chirped CCBG. (a) Schematic of a chirped CCBG. (b) Relative permittivity modulation distribution along the cable. (c) The grating period as a function of period order.

The transmission spectrum ( $S_{21}$ ) can also be calculated by

$$S_{21} = \left( F_{11} - \frac{F_{12} \cdot F_{21}}{F_{22}} \right) e^{-j\beta L}. \quad (8)$$

According to the discussion above, the reflection spectrum of a coaxial cable device is uniquely determined by the coupling coefficient, as given in Eq. (4). There are different approaches to introducing an impedance discontinuity in a coaxial cable, thus generating a partial reflection of the EM wave. Cascading the discontinuities, a grating structure is formed. In this paper, a more general situation is considered, where the permittivity at the discontinuity is  $\epsilon_1$ , and the permittivity of the dielectric layer of the coaxial cable is  $\epsilon_2$ . Thus, Eq. (4) can be simplified as

$$K = \omega(\epsilon_2 - \epsilon_1) \frac{\eta_\mu}{2}, \quad (9)$$

where  $\eta_\mu$  is the wave impedance for the TEM mode and is given by  $\eta_\mu = \sqrt{\mu/\epsilon}$ , where  $\mu$  and  $\epsilon$  are the permeability and permittivity of the medium. Once the coupling coefficient and the spatial distribution of the impedance discontinuities are determined, both the reflection and transmission spectra of the device can be numerically calculated based on Eqs. (7) and (8). In this work, we will focus on the investigation of the reflection spectrum. Calculations

are performed using MATLAB 2018b, installed on a PC with 8 GB of RAM and running Windows 10.

### III. NUMERICAL CALCULATIONS AND DISCUSSION

#### A. Uniform CCBG

Let us start with the uniform CCBG, as schematically shown in Fig. 3(a). Impedance discontinuities are introduced at periodic distances along the axial direction of a coaxial cable. Figure 3(b) illustrates the changes in relative permittivity of the dielectric layer with respect to spatial position along the cable. Reflections occur at each impedance discontinuity, resulting in a resonant pattern in the reflection spectrum of the uniform CCBG. Figure 4(a) shows the calculated reflection spectrum of a CCBG with a uniform grating period of 50 mm and a total of 30 periods. The relative permittivity of the coaxial cable dielectric is set to 2.25 with a loss tangent of 0.0001. The relative permittivity at the discontinuity position is set to 1.75, corresponding to a modulation index of 0.5. The size of an individual discontinuity is 1 mm in width, and the mesh size in the calculation is 1 mm along the axial direction. Discrete resonances can be observed in the observation bandwidth (from 0.001 to 7 GHz) at 1.994, 3.998, and 5.982 GHz, including the fundamental resonance and its harmonics. The obtained resonant frequencies match well with Eq. (2). The reflection at the resonant frequencies increases with increasing frequency, which is due to the fact that the reflection coefficient at each discontinuity increases with increasing frequency, according to Eq. (9). Sidelobes around each resonant frequency are also observed. Figure 4(b) shows the calculated transmission spectrum of the same CCBG. The dip positions in the transmission spectrum match well with the peak positions in the reflection spectrum, as expected. Also, the higher the resonant frequency, the smaller the transmission is. An overall down-trend can be observed in the transmission spectrum due to the introduced loss in the calculation. The discrete dips in the transmission spectrum make the CCBG a potential candidate for notch filtering applications. The attenuation at the resonant frequencies can be adjusted by the number of periods and permittivity modulation strength at discontinuity positions, as it will be shown later.

Figures 4(c) and 4(d) give the reflection and transmission spectra centered at the resonant frequency with different numbers of periods. In the calculation, the grating period and the permittivity modulation were 50 mm and 0.5, respectively. As can be seen, the larger the number of periods, the larger/smaller the reflection/transmission at the resonant frequency, which matches well with the FBG theory.<sup>5</sup> The quality factor (Q-factor) of the reflection/transmission band also increases with the number of periods. The influences of relative permittivity modulation on the reflection and transmission spectra are also investigated and the results are shown in Figs. 4(e) and 4(f). In the calculation, the grating period and the number of periods were 50 mm and 30, respectively. The reflection/transmission increases/decreases as the modulation in relative permittivity of the discontinuity increases. The resonant frequency also shows small shifts due to the change in the effective relative permittivity of the CCBG. Note that larger permittivity modulation can be achieved by partially shorting the inner conductor and outer conductor of the coaxial cable to form a reflector with high

Downloaded from http://pubs.aip.org/jap/article-pdf/doi/10.1063/5.0148559/1696633/164503\_1\_5.0148559.pdf



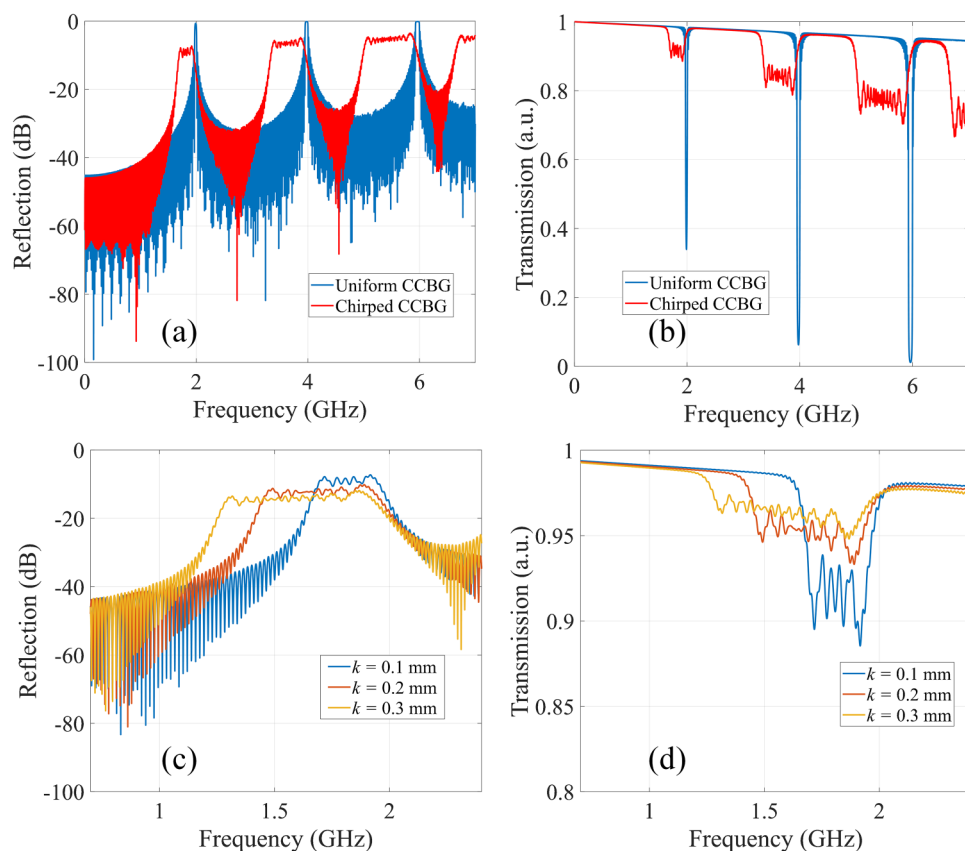


**FIG. 6.** Numerical investigation results of the chirped CCBG. (a) Reflection spectra and (b) transmission spectra comparison between a chirped CCBG and a uniform CCBG with 100 periods. (c) Reflection spectra and (d) transmission spectra of chirped CCBGs with different spatial chirp coefficients.

reflectivity, thus improving the total reflection at the resonance frequencies.<sup>17–19</sup>

The uniform CCBG has been demonstrated as a point strain gauge by taking advantage of the dependence of its resonance frequencies on the period of the grating.<sup>14,15</sup> However, quasi-distributed strain mapping still needs to be further investigated

based on the multiplexing technique used in FBG multiplexing. On the other hand, mimicking the application of FBG in the fiber laser field as an optical mirror, a microwave “laser” configuration, i.e., “maser,” could be developed.<sup>20</sup> The maser system can be used to fast demodulate the resonant frequency of the CCBG; thus, real-time strain monitoring can be realized.

### B. Chirped CCBG

As schematically illustrated in Fig. 1(b), a typical chirped FBG is fabricated by varying the period of the refractive index modulation along the fiber grating length. Due to the variation of the grating period, a broader band is obtained in the reflection/transmission spectrum, corresponding to the varying Bragg wavelengths along the grating length. The unique property of chirped FBGs has enabled important applications in optical communications as dispersion compensators.<sup>21</sup> Very recently, chirped FBGs have also attracted great interest in sensing applications. In this section, the chirped FBG concept is implemented on a coaxial cable, i.e., the chirped CCBG. Figures 5(a) and 5(b) present a schematic diagram of a chirped CCBG and the relative permittivity modulation in a chirped CCBG as a function of spatial position along the axial direction, respectively. The grating period increases linearly with a chirp coefficient  $k$ , as shown in Fig. 5(c). As the grating period

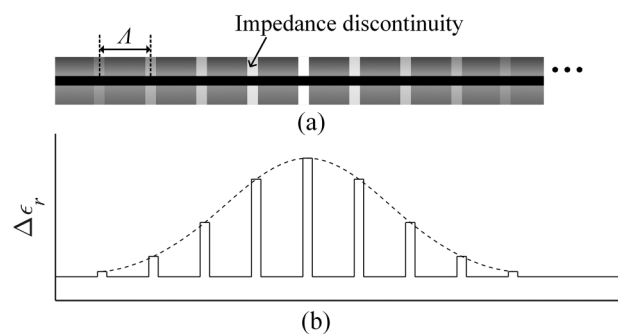


**FIG. 7.** Illustration of a Gaussian-apodized CCBG. (a) Schematic. (b) Relative permittivity modulation varies along the coaxial cable, following the Gaussian apodization profile.

Downloaded from http://pubs.aip.org/jap/article-pdf/doi/10.1063/5.0148559/1696633/164503\_1\_5.0148559.pdf

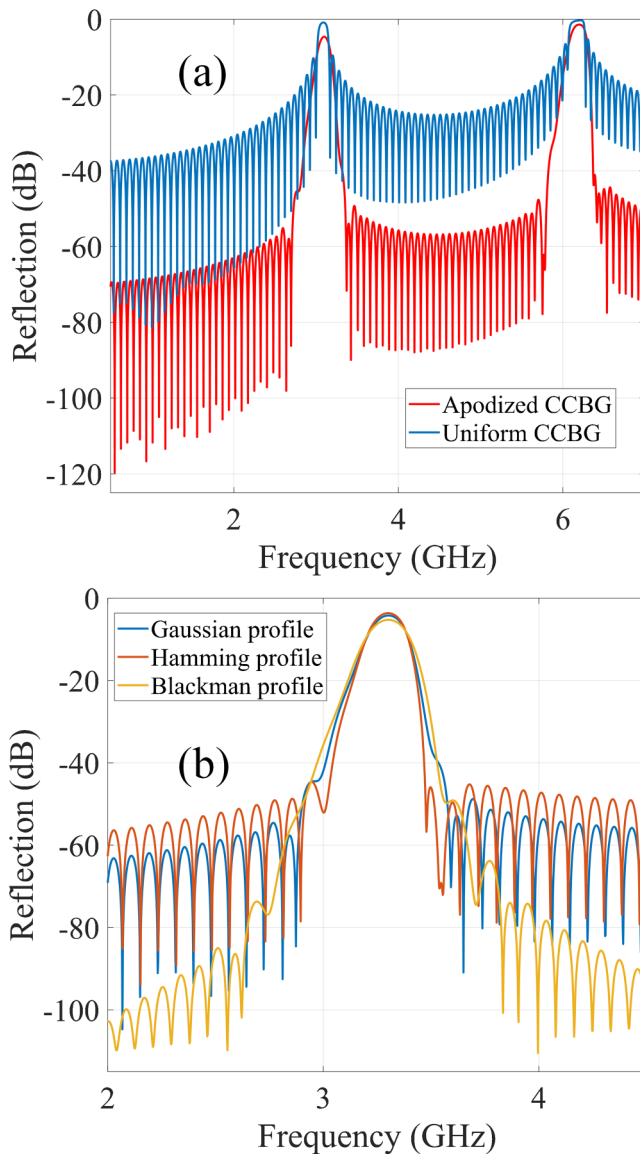


**FIG. 8.** Numerical investigation results of the apodized CCBG. (a) Calculated reflection spectrum of a Gaussian-apodized CCBG compared to a uniform CCBG. (b) Reflection spectra of apodized CCBGs with different apodization profiles.

increases along the axial direction of the coaxial cable, the resonance frequency of the CCBG will decrease accordingly, as predicted by Eq. (2). Thus, broadened and relatively flat resonance bands are expected in the reflection/transmission spectra of a chirped CCBG.

Figures 6(a) and 6(b) show the calculated reflection and transmission spectra of a chirped CCBG with 100 periods. The reflection and transmission spectra of a uniform CCBG are also included for

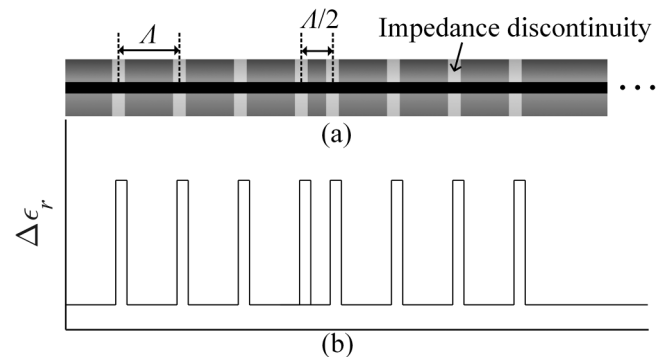


**FIG. 9.** Illustration of a  $\pi$ -phase shifted CCBG. (a) Schematic diagram. (b) Permittivity modulation along the grating length.

comparison. In the calculation, the initial grating period ( $\Lambda$ ) is 50 mm, and the chirp coefficient  $k$  is 0.1 mm. The relative permittivity of the discontinuity is 1, corresponding to a permittivity modulation index of 1.25. The mesh dimension in the calculation is decreased down to 0.1 mm. As can be observed in Figs. 6(a) and 6(b), in comparison with the uniform CCBG, broader reflection and transmission bands are sustained in the chirped CCBG spectra. The continuous increase in the grating period results in resonant frequencies shifting to the lower frequency region, which matches well with the chirped FBG theory. The reflection/transmission at resonant frequencies decreases/increases due to the broadened reflection/transmission band. Figures 6(c) and 6(d) show the influence of the chirp coefficient on the reflection and transmission spectra around the resonant frequency; the larger the chirp coefficient, the broader the reflection/transmission band is. The reflection/transmission also decreases/increases as the reflection/transmission band is broadened. As an analogy to the chirped FBG, the chirped CCBG could also find applications in the sensing field. Differing from a uniform CCBG with a narrow-band reflection, the resonant frequencies in a broad band in a chirped CCBG depend not only on the strain or temperature applied on the grating length but also on the local perturbations along the grating length (i.e., on different sections of the grating). Thus, a chirped CCBG can be used to detect localized perturbations. In this way, the chirped CCBG for sensing applications can potentially solve the issues of long gauge length (i.e., low spatial resolution) faced by a uniform CCBG.

### C. Apodized CCBG

Apodization is a widely used technique in FBGs for depressing the sidelobes in the reflection spectrum.<sup>22</sup> The index modulation strength along an apodized FBG varies along the grating length, as shown in Figs. 1(c) and 1(d). Due to the suppressed sidebands, an apodized FBG is an ideal candidate for bandpass filtering applications. Different apodization profiles have been implemented onto FBGs, such as Gaussian profile, Blackman profile, and Hamming profile.<sup>23</sup> Here, the implementation of apodization to a uniform CCBG is investigated, forming the apodized CCBG. Figure 7(a)



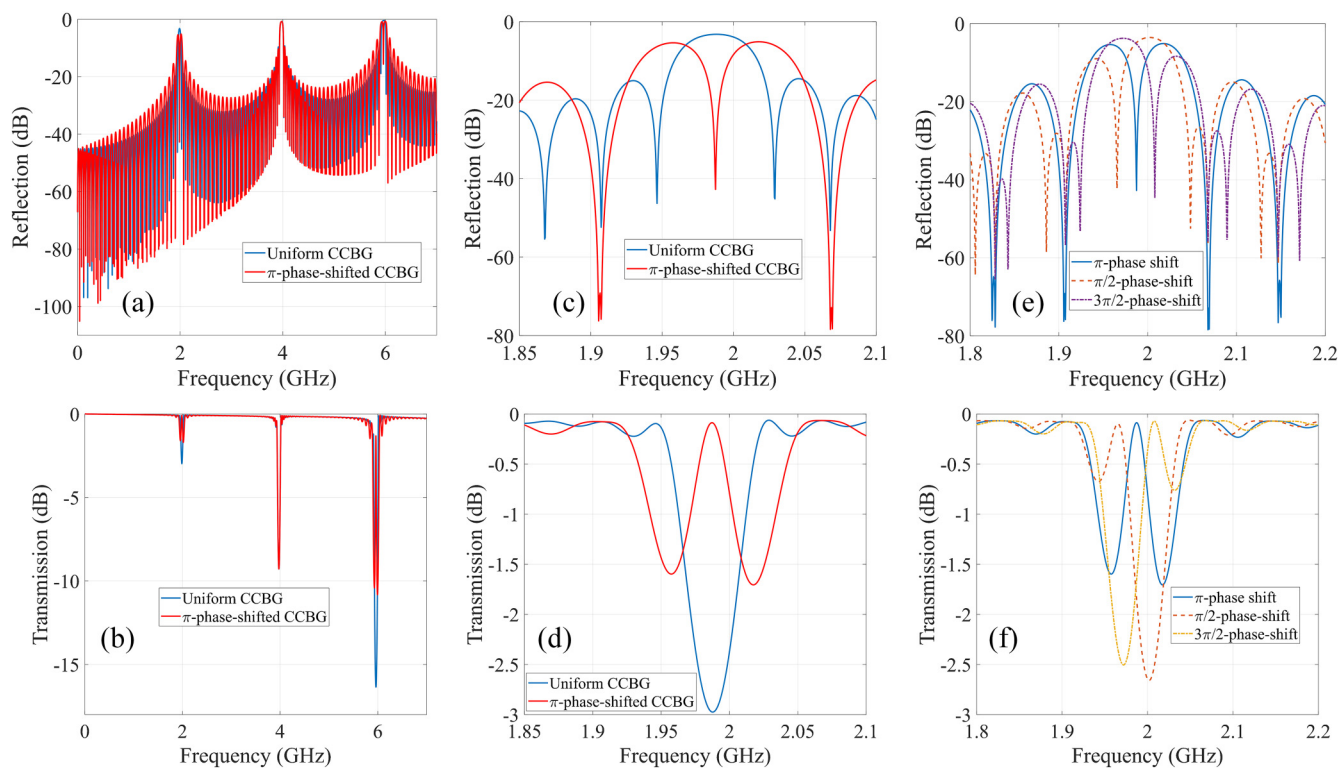


**FIG. 10.** Numerical investigation results of the phase-shifted CCBG. (a) Reflection spectrum and (b) transmission spectrum of a  $\pi$ -phase shifted CCBG compared to a uniform CCBG. Enlarged view of the (c) reflection spectra and (d) transmission spectra centered around fundamental resonance. (e) Reflection spectra and (f) transmission spectra centered around the fundamental resonance of phase-shifted CCBGs with different phase shifts in the permittivity modulation.

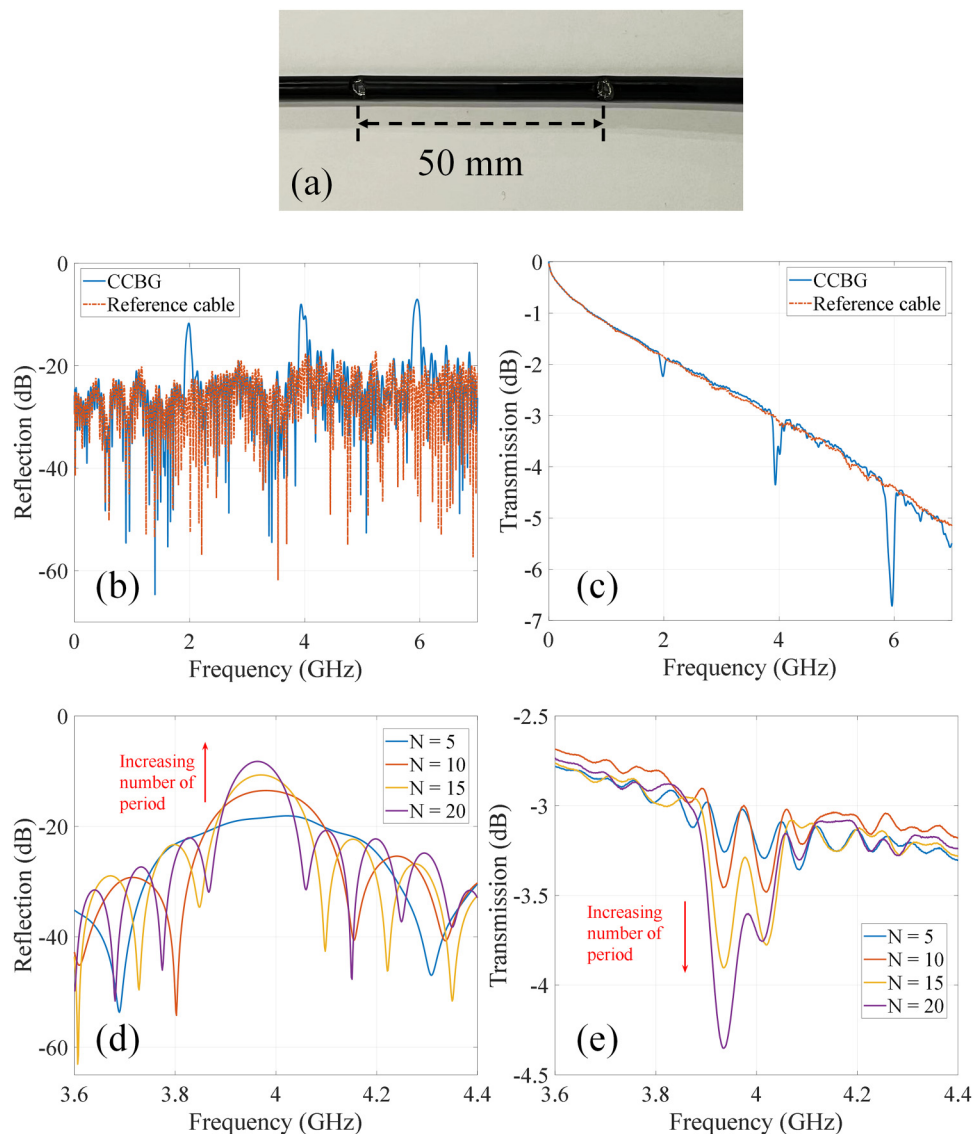
shows a schematic diagram of an apodized CCBG, where the relative permittivity modulation strength varies along the axial direction of the coaxial cable. Figure 7(b) gives the permittivity modulation as a function of the spatial position along the grating length. The dashed line depicts the Gaussian apodization profile. Different profiles can also be applied, as in the case of apodized FBGs.

Figure 8(a) plots the calculated reflection spectra of a uniform CCBG with 40 periods and its Gaussian-apodized form. The period of the grating is set to be 32 mm, and the permittivity modulation strength of the uniform CCBG is 1.25. The meshing dimension used in the calculation is 1 mm. Clearly, the sidelobes are efficiently depressed with an amplitude of  $>30$  dB in the reflection spectrum of the apodized CCBG. Both the reflectivity at the resonant frequency and the Q-factor decrease due to the fact that the total reflection along the grating decreases. The reflectivity and Q-factor can be further improved by increasing the periods and the permittivity modulation strength. The signal-to-noise ratio (SNR) after apodization reaches up to 40 dB, indicating that the apodized CCBG could be potentially used as a bandpass filter. The passband can be adjusted by applying strain or temperature variations to the device since the resonant frequency is sensitive to the two parameters. Meanwhile, the high SNR of the signal is also desired in

sensing applications, which offers a better measurement performance. Figure 8(b) shows the calculated reflection spectra of apodized CCBGs with different apodization profiles, including Gaussian apodization, Hamming apodization, and Blackman apodization. Different apodization profiles result in different characteristic reflection spectra. For instance, it shows that the Blackman apodization has the highest depression for the sidelobes, but with a lower Q-factor. According to different application purposes, the apodized CCBG could be flexibly designed.

#### D. Phase-shifted CCBG

A phase-shifted FBG is fabricated by introducing a phase shift into the period index modulation of a uniform FBG. For instance, a  $\pi$ -phase shifted FBG is realized by splitting a uniform FBG into identical sub-FBGs, where the space between the two sub-FBGs is half-period (i.e.,  $\pi$ -phase difference). The two sub-FBGs are highly reflective and can be conceptually considered as two mirrors of a Fabry-Pérot (FP) etalon. Due to the high reflectivity of the sub-FBGs, the Q-factor of the FP interference is extremely high, resulting in an ultra-narrow band (e.g., few picometers) in the middle of the reflection/transmission spectrum. Therefore, a tailored spectrum with an extremely sharp notch is obtained. The



**FIG. 11.** Experimental validation of the uniform CCBG. (a) Photograph of a part of the prototype CCBG, showing the period of 50 mm. (b) Measured reflection spectrum. The reflection and transmission of a reference cable are also included for comparison. (c) Measured transmission spectrum. (d) Filtered reflection spectrum centered at  $\sim 4$  GHz for different numbers of period. (e) Measured transmission spectrum centered at  $\sim 4$  GHz for different numbers of period.

unique characteristic of phase-shifted FBGs has enabled important applications in distributed feedback lasers and wavelength division multiplexing.<sup>24,25</sup> On the other hand, due to the extremely narrow spectral notch, phase-shifted FBGs have also found successful applications in sensing, e.g., ultrasonic detection with high sensitivity and high resolution.<sup>26</sup> Inspired by the optical counterpart, we implement the phase shift concept to a uniform CCBG, generating the phase-shifted CCBG. Figure 9 illustrates a  $\pi$ -phase shifted CCBG, including a schematic shown in Fig. 9(a) and an illustration of the relative permittivity modulation along the grating length given in Fig. 9(b). Following the same theory of a  $\pi$ -phase shifted FBG, two sub-CCBGs are separated by half grating period.

Figures 10(a) and 10(b) present the calculated reflection spectra and transmission spectra of a  $\pi$ -phase shifted CCBG and a

uniform CCBG with a grating period of 50 mm and a total grating period of 50. The relative permittivity modulation is 1.25. Sharp notches are observed in the fundamental resonant frequency and the third harmonic in both reflection and transmission bands, as expected, while little changes are observed at the second harmonic. Figures 10(c) and 10(d) show an enlarged view of the reflection spectra and transmission spectra at the fundamental resonant frequency, respectively, for clarity. The Q-factor of the sharp notches in the spectra of phase-shifted CCBG is significantly larger than that of the uniform CCBG. The Q-factor of the notch can be further increased by increasing the periods of the grating. Figures 10(e) and 10(f) plot the calculated reflection spectra and transmission spectra of CCBGs with different phase shifts, i.e.,  $\pi$ ,  $\pi/2$ ,  $3\pi/2$ . As can be seen, the notch frequency at both reflection

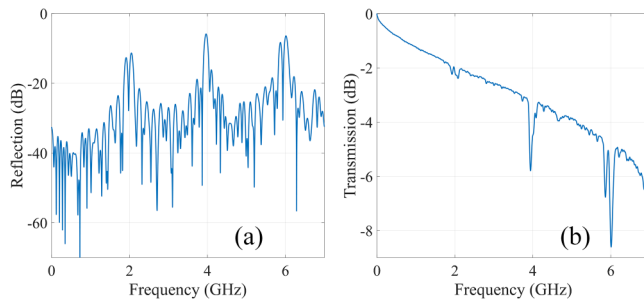


**FIG. 12.** Experimental validation of the  $\pi$ -phase-shifted CCBG. (a) Measured reflection spectrum. (b) Measured transmission spectrum.

and transmission spectra changes as the shifted phase varies, indicating that the notch frequency can be tailored by adjusting the shifted phase for different applications. Due to the tailorable narrow spectral notch, the phase-shifted CCBG could find applications in the RF signal processing field. Besides, the phase-shifted CCBG can also be used for sensing applications. Compared to a uniform CCBG, the phase-shifted CCBG can provide higher measurement sensitivity and higher measurement resolution by tracking the shift of the narrow notch in the spectrum.

#### IV. PROOF OF CONCEPT

A few prototypes of CCBGs were fabricated in the lab to verify the simulation results shown above. Uniform CCBGs were first demonstrated. The coaxial cable used to fabricate the prototype devices is RG 58/U with a length of 2 m. Multiple V-shaped grooves were made along a coaxial cable line by cutting off a part of the dielectric layer using a knife, as shown in Fig. 11(a). Note that the groove-cutting approach is simple but makes it challenging to quantify the local dielectric modulation index due to the irregular shape induced by manual operation. Thus, we were only able to qualitatively verify the simulation results. The distance between two consecutive grooves was 50 mm, i.e., the period of 50 mm. Devices were characterized using a vector network analyzer. Continuous RF signals were used as the probing signal, and the scattering parameters (S11 and S21) were characterized. The input end and the output end of the device were approximately 0.5 m away from port 1 and port 2 of the network analyzer, respectively. The measured reflection spectrum and transmission spectrum of a prototype CCBG with 20 periods are given in Figs. 11(b) and 11(c), respectively. Discrete peaks and dips are observed in the reflection and transmission spectra, respectively, as expected. The resonance frequencies and the overall trend of the curves match well with the results shown in Figs. 4(a) and 4(b). The obvious downward trend shown in Fig. 11(c) is due to the higher transmission loss of the coaxial cable at higher frequencies. The influence of the number of period on the reflection and transmission spectra were also investigated, as shown in Figs. 11(d) and 11(e). The results agree with the simulations given in Figs. 4(c) and 4(d). Thus, the results presented in Fig. 11 verify the effectiveness of the coupled mode theory-based modeling of the CCBG.

A  $\pi$ -phase-shifted CCBG was also fabricated with a period length of 50 mm and a total of 20 periods. The measured transmission and reflection spectra are shown in Figs. 12(a) and 12(b), respectively. Sharp notches are observed, matching well with the simulation results shown in Figs. 10(a) and 10(b). A slight deviation of the notches from the middle of the peak/dip can also be observed, which is due to the fabrication error where the space between the two sub-CCBGs was not exactly half the period. Note that due to the limitation of lab facilities, we were not able to precisely control the permittivity modulation strength and the period so the chirped CCBG and apodized CCBG were not experimentally verified.

#### V. CONCLUSION

Inspired by the well-known FBG, the coaxial cable Bragg grating (CCBG) was proposed as a strain gauge with large strain capability, which has found successful applications in SHM. In this paper, the implementations of FBG techniques on coaxial cables are further investigated. Different special types of CCBGs are proposed and numerically investigated, including chirped, apodized, and phase-shifted configurations. The reflection and transmission spectra of these special types of CCBGs are numerically studied based on the coupled mode theory. The calculation results of the CCBGs match well with the FBG theories. It is shown that the reflection and transmission spectra of a uniform CCBG can be flexibly tailored by introducing the quasi-periodic permittivity modulations along the grating length. The proposed special types of CCBGs can be used for sensing applications with better performance due to the tailored spectrum. Besides, the special types of CCBGs could find potential applications in RF signal processing, bandpass filtering, and communication fields. Note that in addition to coaxial cables, the concept of the Bragg gratings, i.e., one-dimensional photonic crystal structures, can also be applied to other types of transmission lines in the radio frequency regime.

#### ACKNOWLEDGMENTS

This work was supported in part by Researchers Supporting Project (No. RSPD2023R654), King Saud University, Riyadh, Saudi Arabia. The work of Chen Zhu was supported by the Research Initiation Project of Zhejiang Lab (No. 2022ME0PI01).

#### AUTHOR DECLARATIONS

##### Conflict of Interest

The authors have no conflicts to disclose.

##### Author Contributions

**Chen Zhu:** Conceptualization (equal); Formal analysis (equal); Funding acquisition (equal); Investigation (equal); Methodology (equal). **Osamah Alsalmán:** Funding acquisition (equal); Methodology (equal). **Jie Huang:** Methodology (equal).

#### DATA AVAILABILITY

The data that support the findings of this study are available from the corresponding author upon reasonable request.

## REFERENCES

- <sup>1</sup>P. J. Winzer, D. T. Neilson, and A. R. Chraplyvy, "Fiber-optic transmission and networking: The previous 20 and the next 20 years," *Opt. Express* **26**(18), 24190–24239 (2018).
- <sup>2</sup>B. Culshaw, "Optical fiber sensor technologies: Opportunities and-perhaps-pitfalls," *J. Lightwave Technol.* **22**(1), 39–50 (2004).
- <sup>3</sup>M. N. Zervas and C. A. Codemard, "High power fiber lasers: A review," *IEEE J. Sel. Top. Quantum Electron.* **20**(5), 219–241 (2014).
- <sup>4</sup>E. Desurvire, J. R. Simpson, and P. C. Becker, "High-gain erbium-doped traveling-wave fiber amplifier," *Opt. Lett.* **12**(11), 888–890 (1987).
- <sup>5</sup>T. Erdogan, "Fiber grating spectra," *J. Lightwave Technol.* **15**(8), 1277–1294 (1997).
- <sup>6</sup>A. D. Kersey *et al.*, "Fiber grating sensors," *J. Lightwave Technol.* **15**(8), 1442–1463 (1997).
- <sup>7</sup>C. Caucheteur, T. Guo, and J. Albert, "Polarization-assisted fiber Bragg grating sensors: Tutorial and review," *J. Lightwave Technol.* **35**(16), 3311–3322 (2017).
- <sup>8</sup>C. Broadway, R. Min, A. G. Leal-Junior, C. Marques, and C. Caucheteur, "Toward commercial polymer fiber Bragg grating sensors: Review and applications," *J. Lightwave Technol.* **37**(11), 2605–2615 (2019).
- <sup>9</sup>K. O. Hill and G. Meltz, "Fiber Bragg grating technology fundamentals and overview," *J. Lightwave Technol.* **15**(8), 1263–1276 (1997).
- <sup>10</sup>A. Martinez, M. Dubov, I. Khrushchev, and I. Bennion, "Direct writing of fibre Bragg gratings by femtosecond laser," *Electron. Lett.* **40**(19), 1170–1172 (2004).
- <sup>11</sup>P. Moyo, J. M. W. Brownjohn, R. Suresh, and S. C. Tjin, "Development of fiber Bragg grating sensors for monitoring civil infrastructure," *Eng. Struct.* **27**(12), 1828–1834 (2005).
- <sup>12</sup>M. Majumder, T. K. Gangopadhyay, A. K. Chakraborty, K. Dasgupta, and D. K. Bhattacharya, "Fibre Bragg gratings in structural health monitoring—Present status and applications," *Sens. Actuators, A* **147**(1), 150–164 (2008).
- <sup>13</sup>J. Huang, T. Wang, L. Hua, J. Fan, H. Xiao, and M. Luo, "A coaxial cable Fabry-Perot interferometer for sensing applications," *Sensors* **13**(11), 15252–15260 (2013).
- <sup>14</sup>J. Huang, T. Wei, X. Lan, J. Fan, and H. Xiao, *Proc. SPIE* **8345**, 83452Z (2012).
- <sup>15</sup>T. Wei, S. Wu, J. Huang, H. Xiao, and J. Fan, "Coaxial cable Bragg grating," *Appl. Phys. Lett.* **99**(11), 113517 (2011).
- <sup>16</sup>S. Wu, T. Wei, J. Huang, H. Xiao, and J. Fan, "Modeling of coaxial cable Bragg grating by coupled mode theory," *IEEE Trans. Microwave Theory Tech.* **62**(10), 2251–2259 (2014).
- <sup>17</sup>M. F. Ahmed, T. Xue, B. Wu, and J. Huang, "High quality factor coaxial cable Fabry-Perot resonator for sensing applications," *IEEE Sens. J.* **17**(10), 3052–3057 (2017).
- <sup>18</sup>C. Zhu, Y. Chen, Y. Zhuang, and J. Huang, "A centimeter-range displacement sensor based on a hollow coaxial cable Fabry-Pérot resonator," *IEEE Sens. J.* **18**(11), 4436–4442 (2018).
- <sup>19</sup>C. Zhu, Y. Zhuang, Y. Chen, B. Zhang, and J. Huang, "Contactless liquid interface measurement based on a hollow coaxial cable resonator," *Sens. Actuators, A* **285**, 623–627 (2019).
- <sup>20</sup>C. Zhu, Y. Tang, J. Guo, R. E. Gerald, and J. Huang, "High-temperature and high-sensitivity pressure sensors based on microwave resonators," *IEEE Sens. J.* **21**(17), 18781–18792 (2021).
- <sup>21</sup>D. Tosi, "Review of chirped fiber Bragg grating (CFBG) fiber-optic sensors and their applications," *Sensors* **18**(7), 2147 (2018).
- <sup>22</sup>T. Komukai, K. Tamura, and M. Nakazawa, "An efficient 0.04-nm apodized fiber Bragg grating and its application to narrow-band spectral filtering," *IEEE Photonics Technol. Lett.* **9**(7), 934–936 (1997).
- <sup>23</sup>A. Syahriar, D. Astharini, and A. H. Lubis, "The effects of apodization profile on uniform fiber Bragg gratings," in *2015 9th International Conference on Telecommunication Systems Services and Applications (TSSA)* (IEEE, 2015), pp. 1–6.
- <sup>24</sup>G. P. Agrawal and S. Radic, "Phase-shifted fiber Bragg gratings and their application for wavelength demultiplexing," *IEEE Photonics Technol. Lett.* **6**(8), 995–997 (1994).
- <sup>25</sup>A. Melloni, M. Chinello, and M. Martinelli, "All-optical switching in phase-shifted fiber Bragg grating," *IEEE Photonics Technol. Lett.* **12**(1), 42–44 (2000).
- <sup>26</sup>A. Rosenthal, D. Razansky, and V. Ntziachristos, "High-sensitivity compact ultrasonic detector based on a pi-phase-shifted fiber Bragg grating," *Opt. Lett.* **36**(10), 1833–1835 (2011).